Journal of Materials Chemistry A

PAPER

View Article Online
View Journal | View Issue

Check for updates

Cite this: J. Mater. Chem. A, 2019, 7, 14079

Efficient solar-driven hydrogen generation using colloidal heterostructured quantum dots†

Kanghong Wang, [ab] Xin Tong, [bc] Yufeng Zhou,[b] Hui Zhang, [b] Fabiola Navarro-Pardo, [bc] Gurpreet S. Selopal, [bc] Guiju Liu,[d] Jie Tang,[d] Yiqian Wang,[d] Shuhui Sun, [b] Dongling Ma,[b] Zhiming M. Wang,[c] François Vidal,[b] Haiguang Zhao, *[d] Xuhui Sun *[a] and Federico Rosei*[bc]

Received 20th March 2019
Accepted 13th May 2019

DOI: 10.1039/c9ta03026c

rsc.li/materials-a

Mesoporous TiO_2 sensitized with colloidal quantum dots (QDs) is considered as a promising system for photoelectrochemical (PEC) hydrogen generation, in view of its low cost and high solar energy to fuel conversion efficiency. On the other hand, the limited long term stability and low current density of this system still hinder its commercialization. Here, we report a CdSe/CdSeS alloy/CdS core/shell/shell QD sensitized mesoporous TiO_2 photoanode, which exhibits high performance and long-term stability for solar-driven hydrogen generation. A gradient CdSe/alloy-shell/CdS core/shell/shell structure is designed to accelerate exciton separation through the band engineering approach. Compared with the common CdSe/CdS core/shell structure, light absorption of QDs containing an intermediate alloyed layer is extended to longer wavelengths and more importantly, the photocurrent density is improved up to 17.5 mA cm^{-2} under one sun illumination (AM 1.5 G, 100 mW cm^{-2}), a record value for PEC cells based on colloidal QDs for hydrogen generation. In addition, the as-fabricated PEC cell shows an unprecedented long-term stability, maintaining 50% of its initial value after continuous operation for over 39 hours, indicating that the gradient core/shell/shell QD based photoanode is a promising candidate for solar-driven hydrogen generation.

Introduction

Harvesting and converting solar energy is an efficient approach to address the energy crisis arising from the ever increasing global demand for energy. Among numerous technologies, solar-driven generation of hydrogen (H_2) has been widely studied.[1–4] Photoelectrochemical (PEC) hydrogen production is a promising approach to split water into H_2 and O_2 under solar irradiation *via* a low-cost, simple and environment-friendly methodology compared to electrical or chemical water splitting. In general, a PEC system consists of a semiconductor based photoanode, a counter electrode and an electrolyte. Until now, metal oxides (*e.g.* TiO_2 and ZnO)[5–7] are the most widely investigated semiconductors as photoanode materials for H_2 evolution due to their high stability against photo/chemical corrosion at neutral or basic pH.[8,9] However, the use of solar light by these metal oxides is quite limited due to their wide band gaps (for example, 3.2 eV of TiO_2),[10,11] which only allows absorbing UV photons, resulting in low solar to H_2 conversion efficiency. Colloidal semiconductor quantum dots (QDs) have been widely used as sensitizers for solar-driven H_2 generation due to their unique optoelectronic properties, such as a size tunable band gap,[12] wide absorption spectra, high absorption coefficients and multiple exciton generation (MEG).[13] Compared to pure metal oxides, QD sensitized metal oxide photoanodes have a broader absorption range which significantly overlaps with the solar spectrum. As such, numerous types of QDs (*e.g.* PbS,[14,15] CdSe,[16–18] CdS,[19–21] and $CuInSe_xS_{1-x}$[22,23]) have been used to fabricate QD sensitized TiO_2 heterostructure photoanodes for efficient PEC H_2 generation. However, the efficiency of PEC cells for H_2 production is still low (solar-to-hydrogen efficiency less than 10%) compared with electrolysis (solar-to-hydrogen efficiency over 30%)[24] and the long-term stability of PEC cells is still significantly lower than target values for commercial applications (few cases reported stability more than one day while commercial devices need thousands of hours), due to the following challenges: (i)

[a]Jiangsu Key Laboratory for Carbon-Based Functional Materials & Devices, Institute of Functional Nano & Soft Materials (FUNSOM), Joint International Research Laboratory of Carbon-Based Functional Materials and Devices, Soochow University, Suzhou, 215123, Jiangsu, China. E-mail: xhsun@suda.edu.cn

[b]Institut National de la Recherche Scientifique, Centre Énergie, Matériaux et Télécommunications, 1650 Boul. Lionel Boulet, J3X 1S2 Varennes, Québec, Canada. E-mail: rosei@emt.inrs.ca

[c]Institute of Fundamental and Frontier Sciences, University of Electronic Science and Technology of China, Chengdu 610054, P R China

[d]State Key Laboratory of Bio-Fibers and Eco-Textiles & College of Physics, Qingdao University, No. 308 Ningxia Road, Qingdao 266071, PR China. E-mail: hgzhao@qdu.edu.cn

† Electronic supplementary information (ESI) available. See DOI: 10.1039/c9ta03026c

Published on 15 May 2019. Downloaded by Qingdao University on 6/14/2019 7:15:06 AM.

Published on 15 May 2019. Downloaded by Qingdao University on 6/14/2019 7:15:06 AM.

inefficient charge (electron/hole pair) separation and transfer caused by fast charge recombination; (ii) the sensitivity of QDs to the surrounding environment, such as temperature, light and moisture, which tends to degrade their properties. Traps and defects that form at the surface of QDs serve as recombination centers for electron and hole pairs,[25–27] which degrade the device performance; in addition, the PEC of the device lacks long-term stability (*i.e.*, stable H_2 generation rate as a function of time) due to the decomposition of QDs caused by the use of strong alkaline electrolytes (pH $\sim$ 13–14).[28]

Colloidal "giant" core/shell QDs (*e.g.* CdSe/CdS and PbS/CdS) consist of a small-sized core (radius less than 2 nm) and thick shell (up to 10 nm). These systems are promising sensitizers for metal oxides (*e.g.* TiO_2) to fabricate photoanodes for PEC hydrogen generation.[15,22,29–31] Compared to bare QDs and thin-shell QDs (shell thickness less than 1.5 nm), "giant" core/shell QDs have several advantages, such as: (i) by selecting semiconducting materials and tailoring the core size and shell thickness, quasi-type II band alignment can be achieved in a giant core/shell QD system in which the electrons can leak into the shell region, while the holes remain confined in the core region.[32,33] The spatial separation of electrons and holes and prolonged photoluminescence (PL) lifetime of excitons in giant QDs are favorable for the separation of electrons and holes and their subsequent respective transfer to the electron/hole (e^-/h^+) acceptors; (ii) the giant QDs are very stable and less sensitive to the surrounding chemical conditions attributed to the efficient isolation of the core from their environments due to the presence of the thick shell.

On the other hand, due to the limited selection of suitable semiconducting materials and synthetic approaches, the absorption of giant QDs (*e.g.* CdSe/CdS,[34] PbS/CdS,[15] and PbSe/CdSe[35]) is governed by the thick shell and the spectral range is typically less than 500 nm. An efficient solution may consist in the introduction of an interfacial layer between the core and shell which leads to the concept of "Alloyed layers" to simultaneously improve the absorption of giant QDs and the efficiency of carrier spatial separation through an interface engineering approach.[36,37]

To date, PEC devices composed of heterostructured giant core/shell QDs of CdSe/CdS with TiO_2 can achieve $\sim$10 mA cm^{-2} photocurrent density under one sun illumination (AM 1.5, 100 mW cm^{-2}).[29] The highest photocurrent density reported so far in Quantum Dot Solar Technologies was $\sim$14.9 mA cm^{-2} based on a CdS/CdSe co-sensitized TiO_2 photoelectrode.[38] Recently, a photoanode based on a CdSe/CdS/TiO_2 nanowire heterostructure was demonstrated, showing a significant enhancement of the photocurrent density up to 16.2 mA cm^{-2}.[39] However, poor stability and a complex synthetic approach still limit its further improvement.

Here we report the facile fabrication of a PEC device using two types of colloidal CdSe/alloyed layers/CdS core/shell/shell QDs (denoted as CdSe/Alloy#1 and CdSe/Alloy#2), used to sensitize a mesoporous TiO_2 film as a composite photoanode material. The QDs were deposited into a mesoporous TiO_2 film by electrophoretic deposition (EPD)[40] to achieve a close contact. Subsequently, two layers of ZnS prepared *via* successive ionic layer adsorption and reaction (SILAR) were overgrown on the TiO_2/QD anode to prevent photocorrosion. Typically, the CdSe core was synthesized *via* a hot-injection approach and then 6 monolayers of CdS were coated on the surface of the CdSe core through SILAR, forming a structure of CdSe/6CdS. Based on this structure, six monolayers of CdS were transformed into $CdSe_xS_{1-x}$ alloyed layers as the shell while keeping the same CdSe core size. The shell of CdSe/Alloy#1 QDs has four monolayers of $CdSe_xS_{1-x}$ ($x = 0.5$) and two monolayers of pure CdS. On the other hand, the shell of CdSe/Alloy#2 QDs consists of five monolayers of $CdSe_xS_{1-x}$ (x varies from 0–1) and one monolayer of CdS. The fabricated PEC system based on the TiO_2/CdSe/Alloy#1/ZnS and TiO_2/CdSe/Alloy#2/ZnS photoanodes exhibited a saturated photocurrent density of $\sim$15.1 mA cm^{-2} and $\sim$17.5 mA cm^{-2} under standard AM 1.5 G solar irradiation (100 mW cm^{-2}), respectively. By adding alloyed layers, a gradient band structure was built to accelerate the carrier transition. This leads to reduced charge recombination, significantly improving the saturated photocurrent density to a value of $\sim$17.5 mA cm^{-2} compared with 6.2 mA cm^{-2} of the PEC device based on CdSe/6CdS QDs. This is a record value for colloidal QD based PEC devices for hydrogen generation. In addition, by optimizing the thickness of the ZnS layer, annealing treatment conditions and SiO_2 coating, the stability performance for the alloyed QD sensitized photoanode is improved significantly. These results suggest that the gradient "giant" core/shell/shell QD structure may be used to realize high efficiency, stable, low-cost solar-driven PEC hydrogen production.

Experimental methods

Materials

Sulfur (100%), oleylamine (OLA) (technical grade, 70%), cadmium oxide (99%), cadmium nitrate tetrahydrate (≥99%), oleic acid (OAc), rhodamine 6G and octadecene (ODE), selenium pellet (≥99.999%), trioctyl phosphine oxide (TOPO), trioctyl phosphine (TOP) (97%), hexane, zinc acetate dihydrate (98%), sodium sulfide nonahydrate (≥99.9%), sodium sulfide (Na_2S), sodium hydroxide, sodium sulfite (Na_2SO_3), toluene, methanol, acetone, ethanol and isopropanol (IPA) were obtained from Sigma-Aldrich Inc. Ti-nanoxide BL/SC was purchased from Solaronix. Titania paste (code18NR-AO) consisting of a blend of active anatase particles (20 nm in diameter) and larger anatase scattering particles (up to 450 nm in diameter) was supplied by Dyesol (Queanbeyan, Australia). Fluorine doped tin oxide (FTO) coated glass substrates with a sheet resistance of 10 Ω per square were purchased from Pilkington glasses. All chemicals were used as received.

Synthesis of CdSe QDs and core/shell QDs

CdSe QDs were synthesized by using the hot injection approach. Typically, TOPO (1 g) and Cd-oleate (0.38 mmol, 1 mL) in 8 mL of ODE were purged with N_2 at room temperature for 30 min. The reaction system was evacuated for 30 min at 100 °C, and then the temperature was raised to 300 °C. The mixture of TOP–Se (4 mmol, 4 mL), 3 mL of OLA, and 1 mL of ODE at room

 This journal is © The Royal Society of Chemistry 2019

Published on 15 May 2019. Downloaded by Qingdao University on 6/14/2019 7:15:06 AM.

temperature was quickly injected into the Cd-oleate suspension under vigorous stirring. The reaction cell was quenched with cold water after injection. Ethanol (20 mL) was added and then the suspension was centrifuged, and the supernatant was removed and finally the QDs were dispersed in toluene.

Deposition of CdS layers on CdSe QDs followed procedures described in the literature.[29] Typically, in a 50 mL round-bottom flask, OLA (5 mL), ODE (5 mL) and CdSe QDs ($\sim 2 \times 10^{-7}$ mol in hexane) were degassed at 110 °C for 30 min. The reaction flask was re-stored with N_2 and the temperature was further raised to 240 °C with stirring. The $Cd(OAc)_2$ dispersed in ODE (0.25 mL, 0.2 M) was added dropwise and the mixture was allowed to react for 2.5 hours, followed by dropwise addition of 0.2 M sulfur in ODE with the same volume. The shell was further annealed for 10 min. All subsequent shells were annealed at 240 °C for ~10 min following the injection of sulfur and ~2.5 hours following dropwise addition of $Cd(OAc)_2$ in ODE. Sulfur/$Cd(OAc)_2$ addition volumes for shell addition cycles 1–6 were as follows: 0.25, 0.36, 0.49, 0.63, 0.8, and 0.98 mL, respectively.

For the growth of the alloyed shell QDs, a mixture of S/Se (different molar ratios of S : Se with a total concentration of 0.2 M) was used for the further growth of the shell until five layers were completed. Subsequently, another CdS layer was coated on the alloyed shell.

The reaction was cooled to room temperature using ice water. Ethanol was added, and then the suspension was centrifuged and the supernatant was removed. The QDs were then dispersed in toluene for further characterization.

Anode preparation

FTO glass substrates were cleaned with Triton, a mixture of methanol, acetone, and IPA (1 : 1 : 2), thoroughly rinsed with deionized water and dried in a N_2 flow. A thin and compact TiO_2 layer was spin coated on FTO glass substrates at 6000 rpm for 30 s by using the solution Ti-Nanoxide BL/SC (Solaronix), followed by annealing in air at 500 °C for 30 min and then cooling to room temperature. Subsequently a commercial TiO_2 paste, a blend of small anatase particles (20 nm in diameter) and larger anatase particles (up to 450 nm in diameter) paste (18NR-AO), was deposited on top of the compact TiO_2 layer by tape casting and dried in air for 20 min. The photoanodes were then heated on a hotplate at 120 °C for 6 min. A second layer of 18NR-AO paste was then deposited on the top, following the same procedure. All thicknesses of the photoanodes were measured by using a profilometer.

EPD of the QDs on the TiO_2 film and further ZnS coating

The as-prepared TiO_2 films on FTO substrates were vertically immersed in a QD dispersion in such a way that the deposited films faced each other. The distance between them was adjusted to be around 1 cm and a direct current (DC) bias of 200 V was applied for 120 min. To wash off unabsorbed QDs after the EPD process, the samples were rinsed several times with toluene and dried with a N_2 flow at room temperature. Prior to ZnS capping, we applied ligand exchange by using two SILAR cycles of methanolic solution cetyl-trimethyl ammonium bromide (CTAB) and toluene for 1 min dipping. The CTAB treated anode was further washed by methanol to remove the chemical residuals from the surface and then dried with N_2, finally one minute dipping in toluene and dried with N_2 for one SILAR cycle. The ZnS capping layer was grown using the SILAR process as follows. In a typical SILAR deposition cycle, Zn^{2+} ions were deposited from a methanolic 0.1 M solution of $Zn(OAc)_2$. The sulfide precursor was 0.1 M solution of Na_2S in a mixture of methanol/water (1/1 v/v). A single SILAR cycle consisted of 1 min dip-coating of the TiO_2 working electrode in the cation precursors (Zn^{2+}) and subsequently in the anion solutions (S^{2-}). After each bath, the photoanode was thoroughly rinsed by immersing it in the corresponding solvent (methanol or mixed solution), respectively, to remove the chemical residuals from the surface and then dried with a N_2 gun. Two SILAR cycles were applied to form the capping ZnS layer.

Vacuum annealing and SiO_2 coating treatment for stability measurements

Photoanodes coated with ZnS were placed inside a vacuum box. The air was pumped out for 30 min. Subsequently, they were annealed at 120 °C for 20 min and cooled down to room temperature. After annealing, SiO_2 coating was carried out by soaking the ZnS capped photoanodes in 0.01 M ethanolic solution of tetraethylorthosilicate for 1 h at 40 °C and then rinsed with ethanol and dried in a continuous nitrogen flow.

ZrO_2 film preparation

ZrO_2 films were prepared using commercial ZrO_2 nanopowder (Aldrich, particle size < 100 nm). A single layer of the ZrO_2 film was deposited on FTO glass by tape casting, and then annealed in air at 500 °C for 30 min and cooled down at room temperature. We studied the electron transfer rate by using transient fluorescence spectroscopy on QDs deposited into TiO_2 or ZrO_2 mesoporous films. The ZrO_2/QD film serves as a benchmark sample, in which the energy levels do not favor electron/hole transfer. The hole transfer rate in this experiment was monitored by immersing the ZrO_2/QD film into a Na_2S/Na_2SO_3 solution (pH ~ 13) as a hole scavenger.

Characterization

Small angle X-ray diffraction (XRD) of extensively purified QDs was carried out with a Philips X'pert diffractometer using a Cu Kα radiation source ($\lambda = 0.15418$ nm). Transmission electron microscopy (TEM), high-resolution transmission electron microscopy (HRTEM) and selected area electron diffraction (SAED) of the QDs and QD-sensitized TiO_2 film were performed by using a JEOL 2100F TEM. A JEOL JSM7401F field emission scanning electron microscope (FE-SEM) equipped with an energy-dispersive X-ray spectrometer (EDS) was used for obtaining the elemental composition within the QD-sensitized TiO_2 film.

The UV-Vis absorption spectra were recorded with a Cary 5000 UV-Vis-NIR spectrophotometer (Varian) with a scan rate of 600 nm min^{-1}. Fluorescence spectra were recorded with

Published on 15 May 2019. Downloaded by Qingdao University on 6/14/2019 7:15:06 AM.

a Fluorolog-3 system (Horiba Jobin Yvon). The PL lifetime of the QDs was measured in the time-correlated single-photon counting (TCSPC) mode with a 444 nm laser. X-ray photoelectron spectroscopy (XPS) was performed using a VG Escalab 220i-XL equipped with a hemispherical analyzer, applying a twin anode X-ray source. The C 1s peak (BE = 284.8 eV) was used as an internal reference to rule out charging effects. The spectra were treated using Casa XPS software (2.3.15 Version).

The theoretical wave functions of electrons and holes were calculated by solving the stationary Schrödinger equation in spherical geometry, in which we used the bulk values for the effective masses of electrons (m_e^*) and holes (m_h^*), namely $m_e^* = 0.44\ m_e$ and $m_h^* = 0.13\ m_e$ for CdSe, and $m_e^* = 0.2\ m_e$ and $m_h^* = 0.7\ m_e$ for CdS, where m_e is the electron mass at rest in a vacuum. The potentials for electrons and holes as a function of position were approximated as the lowest unoccupied molecular orbital (LUMO) and highest occupied molecular orbital (HOMO) levels, respectively, for the bulk materials. For CdSe, these levels are −3.71 and −5.81 eV, respectively, while for CdS they are −3.3 and −5.8 eV, respectively. Outside the QDs, the potentials were set as 0 and −9.8 eV for electrons and holes, respectively. The interaction between electrons and holes was neglected in the calculations.

The PEC performance of the photoelectrodes was evaluated in a typical three-electrode configuration, consisting of a QD-sensitized TiO_2 thick film working electrode, a Pt counter electrode, and a saturated Ag/AgCl reference electrode. A Cu wire was used to connect FTO with the outer circuit. Insulating epoxy resin was used to cover the sample's surface except for the active area, to avoid any direct contact between the electrolyte and the conducting back-contact and/or the connecting wire. Subsequently the sample was fully immersed in the electrolyte containing 0.25 M Na_2S and 0.35 M Na_2SO_3 (pH ∼ 13) as a sacrificial hole scavenger. All potentials, measured with respect to the reference electrode of Ag/AgCl during the PEC measurements, were converted to a scale according to the following equation:

$$V_{RHE} = V_{Ag/AgCl} + 0.197 + pH \times (0.059)$$

The photo-response was measured by using a 150 W Xenon lamp as the light source with an AM 1.5 G filter. The sample was placed at a distance of 20 cm from the lamp. Prior to each measurement, the light intensity was monitored using a thermopile and adjusted to 100 mW cm^{-2}. All the current *versus* potential measurements were carried out at a 20 mV s^{-1} sweep rate.

The wavelength-dependent incident photon-to-current efficiency (IPCE) was calculated according to the following equation:

$$IPCE(\%) = \frac{1240J}{\lambda \times I} \times 100\%$$

where J represents the photocurrent density (mA cm^{-2}), λ is the wavelength of the incident light (nm), and I is the intensity of the incident light (mW cm^{-2}).

Results and discussion

Structure and characterization

The CdSe QD cores were synthesized *via* a hot-injection approach.[41] For the shell growth, SILAR[42] was applied to synthesize the CdSe/CdS core/shell QDs and CdSe/alloy-shell/CdS core/shell/shell QDs. By varying the molar ratio of Se and S for the alloyed layers with identical SILAR cycles, two types of CdSe/alloy-shell/CdS core/shell/shell QDs, denoted as CdSe/Alloy#1 (CdSe/$(CdSe_{0.5}S_{0.5})_4$/$(CdS)_2$) and CdSe/Alloy#2 (CdSe/$(CdSe_xS_{1-x})_5$/CdS), were obtained. The feeding ratio of Se and S for the shell growth is shown in Table 1. After the synthesis of core/shell/shell QDs, 2 layers of ZnS were applied to prevent photocorrosion through SILAR.

In Fig. 1(a)–(c), the TEM images show that the QDs have a uniform size. The cartoons in the inset of the TEM images display the designed structure of the QDs. The average CdSe core diameter and shell thickness are shown in Table 2. In the CdSe/CdS QDs, six monolayers of CdS were coated on the CdSe core (3.3 nm in diameter) with a shell thickness of 1.96 nm, which is consistent with the TEM images. By tuning the feeding ratio of Se and S precursors, CdSe/Alloy#1 and CdSe/Alloy#2 QDs with 2.07 nm and 2.50 nm in shell thickness, respectively, were obtained. The thicker shell for CdSe/Alloy#1 and CdSe/Alloy#2 giant QDs compared to CdSe/6CdS is due to the addition of elemental Se in the shell.[35] In brief, the overall diameters of the as-synthesized alloyed QDs are 7.7 ± 0.8 nm for CdSe/Alloy#1 QDs and 7.9 ± 0.9 nm for CdSe/Alloy#2 QDs, respectively. And for CdSe/6CdS QDs, the final diameters are 7.2 ± 0.5 nm and the overall size distribution of the three types of QDs is shown in Fig. S1.†

From XRD patterns (Fig. S2†), the crystalline structure of the CdSe core in the CdSe/CdS QDs is ascribed to the zinc blende (ZB), while the CdS shell refers to the wurtzite (WZ) crystal structure.[40] For the alloyed QDs (CdSe/Alloy#1 and CdSe/Alloy#2 QDs), the diffraction patterns show that the shell is a mixture of ZB and WZ structures of CdSe(S). In Fig. 1(d), the HRTEM image shows the crystal lattice of CdSe/Alloy#2 QDs which indicates high crystallinity with lattice fringes. The lattice spacing (d = 3.51 Å) corresponding to the (111) plane of the ZB crystal structure of CdSe is consistent with SAED (Fig. S3†) and XRD patterns. Fig. 1(e) shows the image of CdSe/Alloy#2 QDs deposited into TiO_2 through EPD in which no obvious aggregation of QDs is observed. XPS results further confirm the existence of elemental Cd, Se and S in the CdSe/Alloy#2 QDs (Fig. S4†). Cross-sectional SEM and EDS were further conducted, supporting the uniform dispersion of the CdSe/Alloy#2 QDs inside the mesoporous TiO_2 film and the ratio of all elements is shown in Fig. S5.†

Table 1 Ratio of Se/S in the shell as a function of SILAR cycle

Sample	1	2	3	4	5	6
CdSe/6CdS	0/10	0/10	0/10	0/10	0/10	0/10
CdSe/Alloy#1	5/5	5/5	5/5	5/5	0/10	0/10
CdSe/Alloy#2	9/1	8/2	7/3	5/5	3/7	0/10

This journal is © The Royal Society of Chemistry 2019

Published on 15 May 2019. Downloaded by Qingdao University on 6/14/2019 7:15:06 AM.

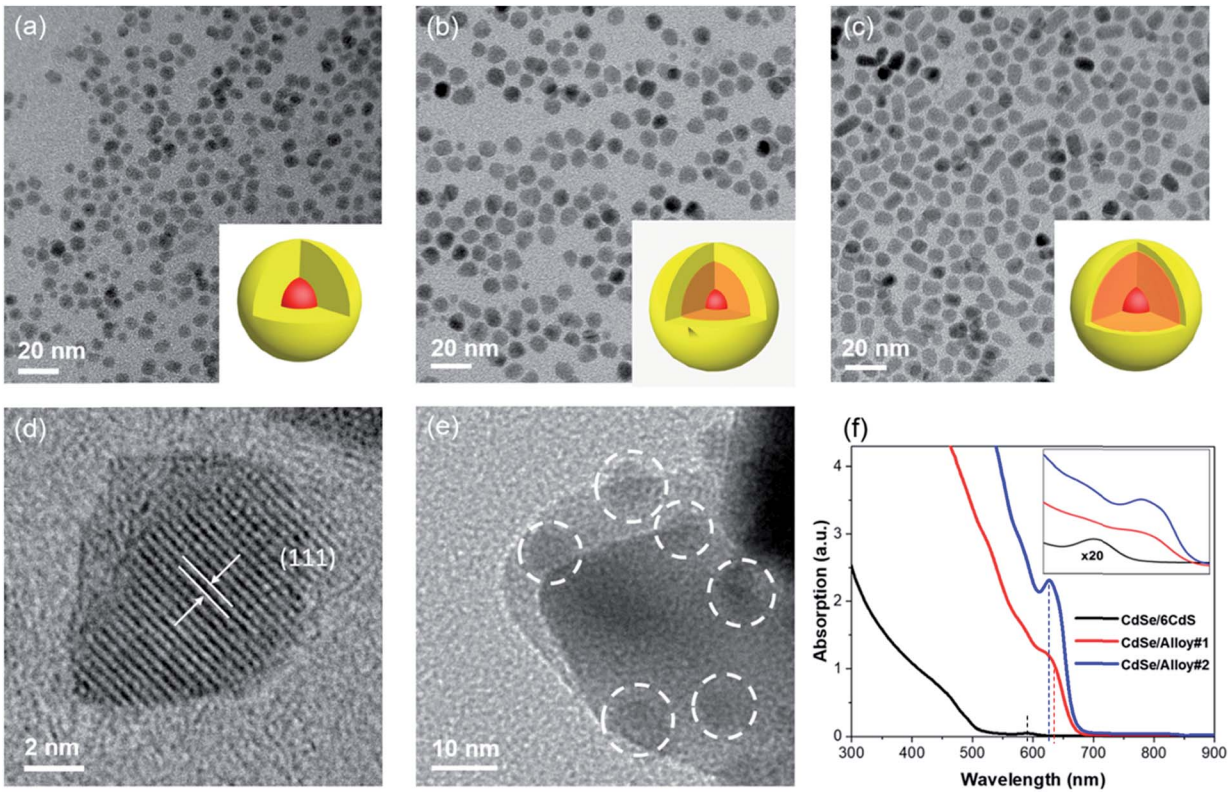

Fig. 1 TEM images and QD structure of (a) CdSe/6CdS; (b) CdSe/Alloy#1; (c) CdSe/Alloy#2; (d) HRTEM image of CdSe/Alloy#2 QDs; (e) CdSe/Alloy#2 QDs in the TiO_2 film; (f) UV-Vis absorption spectra of QDs in toluene. Inset shows the magnified absorption spectra of QDs in solution, where the corresponding first exciton absorption peaks are clearly seen.

Table 2 Optical and size parameters of the as-synthesized core/shell and core/shell/shell QDs in toluene and QDs deposited on the TiO_2 mesoporous film

Sample	D^a (nm)	H^b (nm)	Abs (nm)	PL (nm)
CdSe/6CdS	3.30	1.96	591	605
CdSe/Alloy#1	3.30	2.07	632	649
CdSe/Alloy#2	3.30	2.50	626	650

[a] D is the CdSe core diameter. [b] H is the shell thickness.

Optical properties of QDs

Fig. 1(f) shows that the first-excitonic absorption peaks for the three types of QDs in toluene are observed at ~591 nm (CdSe/6CdS), 632 nm (CdSe/Alloy#1), and 626 nm (CdSe/Alloy#2), respectively. These results are consistent with the PL spectra presented in Fig. S6.† With the presence of interfacial alloy layers, the absorption of QDs is shifted to longer wavelengths due to the narrow band gap of CdSe compared to CdS and the quantum size effect related to the increased size.[43] At the same time, the PL peak is observed to red shift due to the leakage of electrons from the core to the shell region.[29] The same PL peak position in both QDs implies the same degree of electron leakage.[36]

Fig. 2(a) shows the band structure and carrier transition of the CdSe/Alloy#2 QD based photoanode. In general, upon solar illumination, photogenerated excitons will dissociate into electron/hole pairs at the QDs/TiO_2 interface. The electrons will leak from the CdSe core to the shell region and will then be injected into the TiO_2 layer due to electronic band bending, and subsequently collected by the FTO electrode. Finally, electrons are transported through an external circuit to the Pt counter electrode for water reduction.[14,30,44,45] Since the conduction band level of CdS is higher than that of CdSe, the gradient band structure serves as a shortcut for electrons to overcome the original high energy barrier, thereby improving the likelihood of electrons to leak from the core to the shell. Meanwhile, the holes are extracted from the Na_2S/Na_2SO_3 electrolyte (pH ~ 13) which serves as a hole scavenger. Benefiting from the gradient band structure of the CdSe/Alloy#2 QDs, the carriers are more likely to transfer from the core to the shell and then out of the QDs with a lower probability for recombination inside the QDs. The band structure and charge transition diagrams of CdSe/Alloy#1 QDs are shown in Fig. S8.† Similar to the CdSe/Alloy#2 QDs, the CdSe/Alloy#1 QDs provide an intermediate layer between the CdSe core and CdS shell and exhibit better charge transfer efficiency compared to CdSe/6CdS QDs. The relatively energy level for CdSe, CdS and TiO_2 are obtained from the literature,[2,29,33] while the energy level for the $CdSe_xS_{1-x}$ alloyed shell is estimated according to the ratio of Se and S.

To further investigate the charge dynamics behavior of the two types of alloyed QDs, TiO_2 and ZrO_2 mesoporous films were used as substrates on which the QDs are deposited. With the

Published on 15 May 2019. Downloaded by Qingdao University on 6/14/2019 7:15:06 AM.

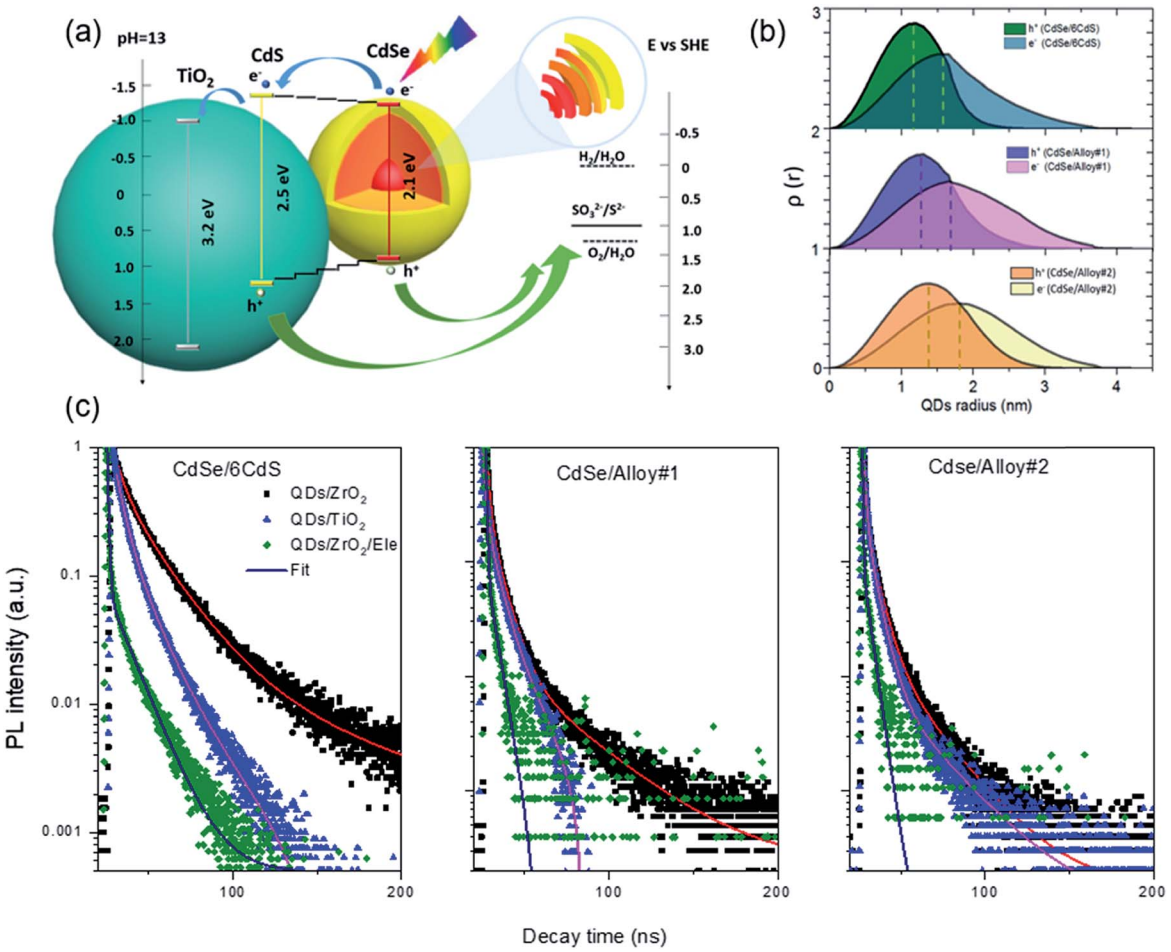

Fig. 2 (a) Schematic diagram of the band structure and carrier transition of the CdSe/Alloy#2 QD based photoanode; (b) spatial probability distribution value $\rho(r)$ of electrons and holes as a function of QD radius (nm) for CdSe/6CdS, CdSe/Alloy#1 and CdSe/Alloy#2 QDs (dashed lines show the positions of the peaks); (c) PL spectra of CdSe/6CdS, CdSe/Alloy#1 and CdSe/Alloy#2 QDs after deposited into TiO_2 films, ZrO_2 films and ZrO_2 films in the presence of an electrolyte.

addition of the electrolyte which serves as a hole scavenger, the hole transfer rate can be calculated and compared to the one without the electrolyte. Due to the band alignment between ZrO_2 and core/shell QDs, ZrO_2 is used as the benchmark, where the charge injection does not occur and PL degradation can only be attributed to charge recombination. The average lifetime $\langle\tau\rangle$ was calculated by using the following equation:[46]

$$\langle\tau\rangle = \frac{a_1\tau_1{}^2 + a_2\tau_2{}^2 + a_3\tau_3{}^2}{a_1\tau_1 + a_2\tau_2 + a_3\tau_3}$$

The electron/hole transfer rate was calculated based on the average lifetime of QDs on different substrates by referring to the following equations:[47]

$$K_{(\mathrm{et})} = \frac{1}{\langle\tau\rangle \mathrm{QDs/TiO_2}} - \frac{1}{\langle\tau\rangle \mathrm{QDs/ZrO_2}}$$

$$K_{(\mathrm{ht})} = \frac{1}{\langle\tau\ \rangle \mathrm{QDs/ZrO_2(electrolyte)}} - \frac{1}{\langle\tau\rangle \mathrm{QDs/ZrO_2}}$$

where K_{et} and K_{ht} are the transfer rate of the electrons and holes, respectively. $\langle\tau\rangle_{\mathrm{QDs/TiO_2}}$ (or electrolyte) and $\langle\tau\rangle_{\mathrm{QDs/ZrO_2}}$ are the average lifetime of QDs on TiO_2, and immersed in the electrolyte and on ZrO_2, respectively. The values of lifetimes and carrier transfer rates are listed in Table 3.

Generally, for the three types of QDs, the hole transfer rates (K_{ht}) are much larger than the electron transfer rates (K_{et}) due to the large driving force (namely, the energy offset between the highest energy level of valence band of QDs and the energy level of $SO_3{}^{2-}/S^{2-}$) from QDs to the electrolyte. However, the degree of carrier dissociation is different in the three QDs (Fig. 2(b)), whereas K_{ht} is three times larger than K_{et} in CdSe/6CdS QDs. In the alloyed QDs, the K_{ht} increases to values up to 3.7 times larger than K_{et} for CdSe/Alloy#1 QDs and 4.3 times larger than that for CdSe/Alloy#2 QDs, respectively. This phenomenon indicates that band alignment was optimized by the alloyed layers which built a favorable band structure for the carriers to separate spatially, leading to fewer charge recombination events.[48–50]

To further verify the process of the carrier dissociation, we calculated the theoretical electron–hole wave functions. The

 This journal is © The Royal Society of Chemistry 2019

Published on 15 May 2019. Downloaded by Qingdao University on 6/14/2019 7:15:06 AM.

Table 3 Lifetime with different substrates and charge transfer rate

Sample	Lifetime with TiO_2 (ns)	Lifetime with ZrO_2 (ns)	Lifetime with an electrolyte (ns)	Electron transfer rate K_{et} (10^7 s^{-1})	Hole transfer rate K_{ht} (10^7 s^{-1})
CdSe/6CdS	15	25	8	2.7	8.5
CdSe/Alloy#1	14	22	7	2.6	9.7
CdSe/Alloy#2	16	23	8	1.9	8.2

electron [$\psi_e(r)$] and hole $\psi_h(r)$] wave functions for the two types of alloyed core/shell/shell QDs and the CdSe/6CdS QDs were calculated by solving the stationary Schrödinger equation in spherical geometry.[29] The calculated spatial probability distribution [$\rho(r)$] of $\psi_e(r)$ and $\psi_h(r)$ as a function of QD radius (nm) is shown in Fig. 2(b). With the addition of alloyed layers, both $\psi_e(r)$ and $\psi_h(r)$ show an increased leakage into the shell region as a consequence of favorable band alignment. According to Table S2,† which shows the e–h spatial overlapping values and Fig. 2(b) (according to the positions of dashed lines), the overlapping values for electrons and holes increase due to improved band alignment. As a result, the carrier recombination could be more severe in alloyed QDs. However, due to the different transfer rates of electrons and holes, more carriers could be transferred outside the QDs which dominates the values of current density.

PEC performance

As a proof-of-concept, the as-prepared QDs (CdSe/6CdS, CdSe/Alloy#1, and CdSe/Alloy#2) were used as photosensitizers for solar-driven hydrogen generation. The PEC performance is shown in Fig. 3(a)–(c). Typically, QDs are deposited onto mesoporous TiO_2 films *via* an EPD process for 120 min. In addition, 2 layers of the ZnS monolayer are coated on photoanodes using the SILAR approach. The PEC cells are measured in the dark and under continuous and chopped illumination (AM 1.5 G, 100 mW cm^{-2}) by using a typical three electrode configuration with a working electrode (QD based photoanode), Ag/AgCl (saturated with KNO_3 solution) reference electrode and Pt counter electrode. The photocurrent density gradually increases when increasing the applied voltage until the saturated current density is obtained, as shown in Fig. 3(a)–(c). A saturated photocurrent density of 6.2 mA cm^{-2} is obtained in the CdSe/6CdS QD based photoanode system under one sun illumination. The PEC device based on CdSe/Alloy#1 QDs shows an enhanced saturated photocurrent density of ~15.1 mA cm^{-2} which is 2.4 times higher than that of the PEC device based on CdSe/6CdS QDs. In addition, CdSe/Alloy#2 QDs with the gradient alloyed shells exhibit a photocurrent density up to 17.5 mA cm^{-2} which is 2.8 times higher than that of the PEC device based on CdSe/6CdS QDs. Lee[38] *et al.* previously fabricated a TiO_2/CdS/CdSe cascade structure with co-sensitization of CdSe and CdS, reporting 14.9 mA cm^{-2} under one sun illumination (the highest photocurrent density at that time). Later Seol[51] *et al.* reported an $IrO_x \cdot nH_2O$ modified CdSe/CdS/ZnO nanowire photoanode for hydrogen generation which yielded a photocurrent density of 13.9 mA cm^{-2} (at 0.6 V *vs.* RHE). Recently, Kim[52] reported an extra-high current density of 22.1 mA cm^{-2} based on a PbS/Mn-doped CdS/TiO_2 electrode. However, the synthesis method of QDs is SILAR which cannot control the size and shape of QDs precisely. Here, our PEC cell with a photoanode based on alloyed QDs exhibits a photocurrent density of 17.5 mA cm^{-2} under one sun illumination (AM 1.5 G, 100 mW cm^{-2}). The higher current density can be attributed to several synergistic effects: (i) with the addition of elemental Se in the alloyed QDs, the absorption range is extended towards longer wavelengths, which in turn enhances efficient transfer from photons to excitons. (ii) Benefiting from the gradient band structure of the TiO_2/shell/core, large numbers of both electrons and holes can be extracted from QDs into TiO_2, thereby contributing to the current density. Due to the efficient hole transfer, hole accumulation and oxidation were largely suppressed. (iii) According to charge dynamics analysis, the spatial separation of electrons and holes increases, limiting opportunities for recombination. To further investigate the effect of the ZnS coating thickness, three and four cycles were applied as post-treatment of the photoanodes. The PEC performance was then measured for three and four cycles of ZnS coating based on the TiO_2/CdSe/Alloy#2 photoanode, which exhibits a decrease of the photocurrent density with an increase of the thickness of ZnS layers (shown in ESI, Fig. S9†). According to the PEC results, too thick ZnS layers will reduce the efficiency of charge transfer which in turn increases the probability of recombination.[29]

We calculated the H_2 evolution rate based on the measured saturated photocurrent density, finding 135 mL cm^{-2} per day and 156 mL cm^{-2} per day for CdSe/Alloy#1 QDs and CdSe/Alloy#2 QDs samples, respectively.

The stability of the PEC device is also an essential factor for H_2 generation. Stability measurements were conducted under continuous one sun illumination. Due to the surface traps and instability of QDs inside the alkaline electrolyte during long term exposure under one sun illumination, the sample CdSe/Alloy#2 QDs–TiO_2 with two cycles of ZnS coating showed a sharp decrease of the current density at the beginning of the stability measurement and maintained 70% of the initial value of current density after 2 hours of measurement (shown in ESI, Fig. S10†). Multiple approaches were used to optimize the stability. Vacuum annealing,[53] thicker ZnS coating and SiO_2 coating were observed to improve the stability. From Fig. 3(d), by comparing 3ZnS samples with and without annealing treatment, it is found that the initial photocurrent of the annealed one increased and was found to be more stable over a two hour measurement period. This observation indicates that annealing

Published on 15 May 2019. Downloaded by Qingdao University on 6/14/2019 7:15:06 AM.

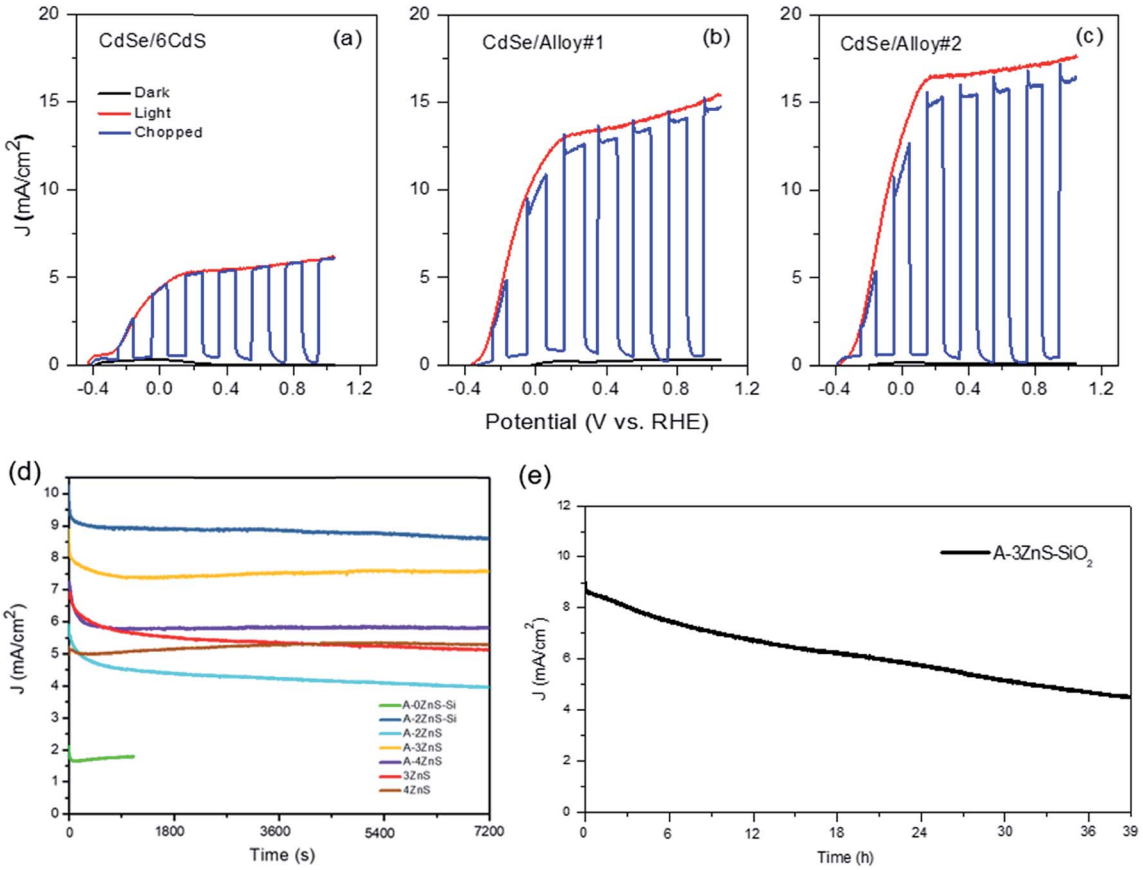

Fig. 3 Photocurrent density-potential dependence of TiO_2 sensitized with (a) CdSe/6CdS QDs; (b) CdSe/Alloy#1 QDs; (c) CdSe/Alloy#2 QDs in the dark (black curve), and under continuous (red curve) and chopped (blue curve) illumination (AM 1.5 G, 100 mW cm^{-2}); stability measurements (photocurrent density as a function of time) of the CdSe/Alloy#2 QD based photoanode at 0.6 V *versus* RHE under AM 1.5 G illumination (100 mW cm^{-2}) (d) with different treatments (annealing and different cycles of ZnS coating and SiO_2 coating) and (e) with annealing-3ZnS–SiO_2 treatment.

is a promising approach to optimize the stability. Two, three and four cycles of ZnS coating were conducted to assess the effect of different ZnS thicknesses. Although the initial current density will decrease with the increase of ZnS cycles (8.8 mA cm^{-2} for the sample with 3 cycles of ZnS coating and 7.2 mA cm^{-2} for the sample with 4 cycles of ZnS coating), similar stability performance as shown in the normalized stability spectra (Fig. S11†) for the thicker ZnS sample was displayed in measurement for 2 hours (86% and 82% of the initial current density was maintained for the samples with 3 and 4 cycles of ZnS coating, respectively). The lower current density values maintained after 2 hours of measurement for the sample with 4 cycles of ZnS coating compared to the one with 3 cycles was attributed to the lower carrier transfer efficiency brought about by the thicker shell. However, the spectra of normalized stability performance (Fig. S11†) showed a better stability trend for longer-term measurement (more than 2 hours). Afterwards, a silica coating was further coated outside the ZnS layers. The sample QDs–TiO_2–2ZnS–SiO_2 showed promising results which simultaneously improved the current density and stability.[54] However, the sample QDs–TiO_2–0ZnS–SiO_2 showed ultra-low current density (~2 mA cm^{-2}) which emphasizes the importance of the ZnS coating and shows that direct SiO_2 coating may destroy the QDs because of the strong base (0.01 M ethanolic solution of tetraethylorthosilicate) during the silica coating process. As the three methods for optimizing the stability all showed an enhancement, the sample with the best conditions (annealing, 3 cycles of ZnS coating and SiO_2 coating) was considered to evaluate the lifetime of the device. As shown in Fig. 3(e) and S13,† CdSe/Alloy#2 QDs–TiO_2 was first annealed, and then coated with 3 layers of ZnS, with or without silica coating. After over 39 hours, the device can still work at 50% of the initial current density value while the sample without SiO_2 coating can operate only for 34 hours at over 50% of its initial value. Due to the wide band gap of SiO_2 (~9 eV),[55] the electrons are largely blocked inside the QDs while the holes can still be extracted by a strong driving force (alkaline electrolyte) where the charge separation can proceed faster. Compared to previous work, which reported a photocurrent density of 13.9 mA cm^{-2},[50] the photoanode of CdSe/CdS/ZnO maintained 50% of the initial value for just three hours. In Adhikari's work,[29] the CdSe/CdS "Giant" QDs only maintain 52% of the initial value after 2 h with 2 layers of ZnS coating while it kept 72% of the initial value with three layers of ZnS coating, yet the current density subsequently dropped to 3.9 mA cm^{-2}, while our PEC cell can maintain 50% of its initial value

 This journal is © The Royal Society of Chemistry 2019

Published on 15 May 2019. Downloaded by Qingdao University on 6/14/2019 7:15:06 AM.

for as long as 39 h, indicating that it can be a promising candidate for long-term stable PEC hydrogen generation. In the future, we will continue working on the optimization of stability performance by tailoring the thickness of ZnS and SiO_2 shells as well as reducing the hole accumulation.

Conclusions and prospects

In summary, we designed a CdSe/alloy shell/CdS sensitized TiO_2 photoanode with a gradient band structure for high-efficiency hydrogen generation. By adjusting the composition of the shell, we obtained a gradient band architecture which leads to an improved charge transfer efficiency. As a result, charge recombination is largely suppressed and the photocurrent density of the alloyed QDs was largely enhanced (up to 17.5 mA cm^{-2}). This is the highest photocurrent density among colloidal QD sensitized TiO_2 photoanodes observed so far. In addition, long-term stable performance was found in the PEC devices based on CdSe/Alloy#2 QDs which can maintain 50% of the initial current density value for over 39 hours under continuous illumination, indicating that they can act as a very stable, efficient and low-cost photoelectrode for H_2 generation with stability comparable to the best stability of PEC devices based on colloidal QDs.

Future directions for PEC cells based on colloidal QDs may focus on engineering the interfacial layer by optimizing its thickness, chemical composition and crystal structure to further improve the performance. Meanwhile, some hole acceptor can be used in the PEC system to improve the hole transfer and further reduce hole accumulation for long-time stability PEC devices.

Author contributions

K. Wang: synthesis and characterization of QDs, PEC measurement, data analysis and manuscript writing. X. Tong and Y. Zhou: XPS characterization, PEC measurement, data analysis, and discussion; H. Zhang: synthesis of QDs, PEC measurement and discussion; F. Navarro Pardo: EDS mapping characterization; G. S. Selopal: TEM characterization and assistance with SiO_2 coating. G. Liu, J. Tang and Y. Wang: TEM measurement and structural characterization of QDs; F. Vidal: simulation of the wavefunctions of QDs; S. Sun, D. Ma, and Z. M. Wang discussed and revised the manuscript; H. Zhao, X. Sun and F. Rosei supervised the work and revised the manuscript.

Conflicts of interest

There are no conflicts to declare.

Acknowledgements

The work was supported by the Natural Science Foundation of China (NSFC) (Grant U1432249), the National Key R&D Program of China (Grant 2017YFA0205002), and the Priority Academic Program Development (PAPD) of Jiangsu Higher Education Institutions. This is also a project supported by the Jiangsu Key Laboratory for Carbon-Based Functional Materials and Devices and Collaborative Innovation Center of Suzhou Nano Science & Technology. F. R. acknowledges funding from the Natural Science and Engineering Research Council of Canada (NSERC) through the discovery grants program (D. M. and F. R.), the Canada Foundation for Innovation (CFI) for infrastructure support and its operating costs and the Fonds de recherche du Québec-Nature et technologies (FRQNT). F. R. is grateful to the Canada Research Chairs program for funding and partial salary support. F. R. also acknowledges the Government of China for a Changjiang scholar short term award and Sichuan Province for a 1000 talents short term award. H. G. Zhao acknowledges the start-up fund from Qingdao University and the funding from the Natural Science Foundation of Shandong Province (ZR2018MB001).

References

1 X. Chen, S. Shen, L. Guo and S. S. Mao, *Chem. Rev.*, 2010, **110**, 6503–6570.
2 M. Gratzel, *Nature*, 2001, **414**, 338–344.
3 Y. Tachibana, L. Vayssieres and J. R. Durrant, *Nat. Photonics*, 2012, **6**, 511–518.
4 S. C. Warren, K. Voitchovsky, H. Dotan, C. M. Leroy, M. Cornuz, F. Stellacci, C. Hebert, A. Rothschild and M. Gratzel, *Nat. Mater.*, 2013, **12**, 842–849.
5 W. Zhou, Z. Yin, Y. Du, X. Huang, Z. Zeng, Z. Fan, H. Liu, J. Wang and H. Zhang, *Small*, 2013, **9**, 140–147.
6 X. Sun, Y. Chu, T. Song, Z. Liu, L. Zhang, X. Wang and Q. Chen, *Solid State Commun.*, 2007, **142**, 15–19.
7 K. Keis, L. Vayssieres, S. E. Lindquist and A. Hagfeldt, *Nanostruct. Mater.*, 1999, **12**, 487–490.
8 M. Ni, M. K. H. Leung, D. Y. C. Leung and K. Sumathy, *Renewable Sustainable Energy Rev.*, 2007, **11**, 401–425.
9 S. U. M. Khan, M. Al-Shahry and W. B. Ingler, *Science*, 2002, **297**, 2243–2245.
10 A. Fujishima and K. Honda, *Nature*, 1972, **238**, 37–38.
11 A. Hagfeldt and M. Gratzel, *Chem. Rev.*, 1995, **95**, 49–68.
12 I. Moreels, Y. Justo, B. D. Geyter, K. Haustraete, J. C. Martins and Z. Hens, *ACS Nano*, 2011, **5**, 2004–2012.
13 A. J. Nozik, M. C. Beard, J. M. Luther, M. Law, R. J. Ellingson and J. C. Johnson, *Chem. Rev.*, 2010, **110**, 6873–6890.
14 L. Jin, B. AlOtaibi, D. Benetti, S. Li, H. Zhao, Z. Mi, A. Vomiero and F. Rosei, *Adv. Sci.*, 2016, **3**, 1500345.
15 L. Jin, G. Sirigu, X. Tong, A. Camellini, A. Parisini, G. Nicotra, C. Spinella, H. Zhao, S. Sun, V. Morandi, M. Zavelani-Rossi, F. Rosei and A. Vomiero, *Nano Energy*, 2016, **30**, 531–541.
16 H. J. Lee, J. H. Yum, H. C. Leventis, S. M. Zakeeruddin, S. A. Haque, P. Chen, S. I. Seok, M. Gratzel and M. K. Nazeeruddin, *J. Phys. Chem. C*, 2008, **112**, 11600–11608.
17 D. Liu and P. V. Kamat, *J. Phys. Chem.*, 1993, **97**, 10769–10773.
18 I. Robel, V. Subramanian, M. Kuno and P. V. Kamat, *J. Am. Chem. Soc.*, 2006, **128**, 2385–2393.

Published on 15 May 2019. Downloaded by Qingdao University on 6/14/2019 7:15:06 AM.

19 H. Gerischer and M. A. Lubke, *J. Electroanal. Chem.*, 1986, **204**, 225–227.
20 S. Kohtani, A. Kudo and T. Sakata, *Chem. Phys. Lett.*, 1993, **206**, 166–170.
21 R. Vogel, K. Pohl and H. Weller, *Chem. Phys. Lett.*, 1990, **174**, 241–246.
22 X. Tong, X. T. Kong, Y. Zhou, F. Navarro-Pardo, G. S. Selopal, S. Sun, A. O. Govorov, H. Zhao, Z. M. Wang and F. Rosei, *Adv. Energy Mater.*, 2018, **8**, 1701432.
23 X. Tong, Y. Zhou, L. Jin, K. Basu, R. Adhikari, G. S. Selopal, H. Zhao, S. Sun, A. Vomiero, Z. M. Wang and F. Rosei, *Nano Energy*, 2017, **31**, 441–449.
24 J. Jia, L. C. Seitz, J. D. Benck, Y. Huo, Y. Chen, J. W. D. Ng, T. Bilir, J. S. Harris and T. F. Jaramillo, *Nat. Commun.*, 2016, **7**, 13237.
25 L. Wu, S. Y. Chen, F. J. Fan, T. T. Zhuang, C. M. Dai and S. H. Yu, *J. Am. Chem. Soc.*, 2016, **138**, 5576–5584.
26 A. P. Alivisatos, *Science*, 1996, **271**, 933–937.
27 Y. Yin and A. P. Alivisatos, *Nature*, 2005, **437**, 664–670.
28 D. Bae, B. Seger, P. C. K. Vesborg, O. Hansen and I. Chorkendorff, *Chem. Soc. Rev.*, 2017, **46**, 1933–1954.
29 R. Adhikari, L. Jin, F. Navarro-Pardo, D. Benetti, B. AIOtaibi, S. Vanka, H. Zhao, Z. Mi, A. Vomiero and F. Rosei, *Nano Energy*, 2016, **27**, 265–274.
30 F. Navarro-Pardo, H. Zhao, Z. Wang and F. Rosei, *Acc. Chem. Res.*, 2018, **51**, 609–618.
31 H. Zhao and F. Rosei, *Chem*, 2017, **3**, 229–258.
32 Y. Chen, J. Vela, H. Htoon, J. L. Casson, D. J. Werder, D. A. Bussian, V. I. Klimov and J. A. Hollingsworth, *J. Am. Chem. Soc.*, 2008, **130**, 5026–5027.
33 S. Brovelli, R. D. Schaller, S. A. Crooker, F. Garcia-Santamaria, Y. Chen, R. Viswanatha, J. A. Hollingsworth, H. Htoon and V. I. Klimov, *Nat. Commun.*, 2011, **2**, 280.
34 B. N. Pal, Y. Ghosh, S. Brovelli, R. Laocharoensuk, V. I. Klimov, J. A. Hollingsworth and H. Htoon, *Nano Lett.*, 2012, **12**, 331–336.
35 B. De Geyter, Y. Justo, I. Moreels, K. Lambert, P. F. Smet, D. Van Thourhout, A. J. Houtepen, D. Grodzinska, C. de Mello Donega, A. Meijerink and D. Vanmaekelbergh, *ACS Nano*, 2011, **5**, 58–66.
36 W. K. Bae, L. A. Padilha, Y. S. Park, H. McDaniel, I. Robel, J. M. Pietryga and V. I. Klimov, *ACS Nano*, 2013, **7**, 3411–3419.
37 Y. S. Park, W. K. Bae, T. Baker, J. Lim and V. I. Klimov, *Nano Lett.*, 2015, **15**, 7319–7328.
38 Y. L. Lee, C. F. Chi and S. Y. Liau, *Chem. Mater.*, 2010, **22**, 922–927.
39 H. S. Han, G. S. Han, J. S. Kim, D. H. Kim, J. S. Hong, S. Caliskan, H. S. Jung, I. S. Cho and J. K. Lee, *ACS Sustainable Chem. Eng.*, 2016, **4**, 1161–1168.
40 L. Jin, H. Zhao, D. Ma, A. Vomiero and F. Rosei, *J. Mater. Chem. A.*, 2015, **3**, 847–856.
41 B. O. Dabbousi, J. Rodriguez-Viejo, F. V. Mikulec, J. R. Heine, H. Mattoussi, R. Ober, K. F. ensen and M. G. Bawendi, *J. Phys. Chem. B*, 1997, **101**, 9463–9475.
42 Y. Ghosh, B. D. Mangum, J. L. Casson, D. J. Williams, H. Htoon and J. A. Hollingsworth, *J. Am. Chem. Soc.*, 2012, **134**, 9634–9643.
43 H. Zhao, D. Benetti, L. Jin, Y. Zhou, F. Rosei and A. Vomiero, *Small*, 2016, **12**, 5354–5365.
44 A. P. Alivisatos, *J. Phys. Chem.*, 1996, **100**, 13226–13239.
45 P. V. Kamat and D. Meisel, *Stud. Surf. Sci. Catal.*, 1997, **103**, 1–3.
46 H. Zhao, Z. Fan, H. Liang, G. S. Selopal, B. A. Gonfa, L. Jin, A. Soudi, D. Cui, F. Enrichi, M. M. Natile and I. Concina, *Nanoscale*, 2014, **6**, 7004–7011.
47 H. McDaniel, N. Fuke, N. S. Makarov, J. M. Pietryga and V. I. Klimov, *Nat. Commun.*, 2013, **4**, 2887.
48 T. X. Ding, J. H. Olshansky, S. R. Leone and A. P. Alivisatos, *J. Am. Chem. Soc.*, 2015, **137**, 2021–2029.
49 M. Cirillo, T. Aubert, R. Gomes, R. Van Deun, P. Emplit, A. Biermann, H. Lange, C. Thomsen, E. Brainis and Z. Hens, *Chem. Mater.*, 2014, **26**, 1154–1160.
50 L. Dworak, V. V. Matylitsky, V. V. Breus, M. Braun, T. Basche and J. Wachtveitl, *J. Phys. Chem. C*, 2011, **115**, 3949–3955.
51 M. Seol, J. W. Jang, S. Cho, J. S. Lee and K. Yong, *Chem. Mater.*, 2013, **25**, 184–189.
52 J. Y. Kim, Y. J. Jang, J. Park, J. Kim, J. S. Kang, D. Y. Chung, Y. E. Sung, C. Lee, J. S. Lee and M. J. Ko, *Appl. Catal., B*, 2018, **227**, 409–417.
53 C. F. Chi, S. Y. Liau and Y. L. Lee, *Nanotechnology*, 2010, **21**, 025202.
54 N. Wang, S. Koh, B. G. Jeong, D. Lee, W. D. Kim, K. Park, M. K. Nam, K. Lee, Y. Kim, B. H. Lee and K. Lee, *Nanotechnology*, 2017, **28**, 185603.
55 J. K. Yang, W. S. Kim and H. H. Park, *Thin Solid Films*, 2006, **494**, 311–314.

This journal is © The Royal Society of Chemistry 2019